Oxidation and Diffusion in Ti-Al-(Mo, Nb) Intermetallics

M. RAMACHANDRAN, D. MANTHA, C. WILLIAMS, and R.G. REDDY

The oxidation resistance of Ti-Al intermetallics is superior to many of their counterparts at high temperatures. High-temperature stability of these intermetallics appears to improve with a ternary alloying addition such as Mo, Nb, *etc*. A detailed analysis of oxidation of the Ti_3Al intermetallics, Ti_3Al-2.9 at. pct Mo and Ti_3Al-1.1 at. pct Nb, in pure oxygen using crystallographic and microscopic techniques is presented here. The alloy containing 1.1 at. pct Nb did not show an improvement in oxidation resistance over the base alloy but that containing 2.9 at. pct Mo showed marked resistance to oxidation. Activation energies of oxidation for both the alloys were comparable with those reported in the literature for similar compositions. TiO_2 and Al_2O_3 were the major phases present in the oxide scales of the oxidized alloys. The crystal orientations from the X-ray diffraction (XRD) patterns and the morphologies from scanning electron microscopy (SEM) were in good agreement and were helpful in further analysis of the oxidation process. The effective diffusion of oxygen in the oxide layers was calculated using the mole fraction of individual oxide and the diffusivity of oxygen in pure oxide. The activation energy for the effective diffusion of oxygen through the oxide layers was determined to be ~24 kJ/mol. The activation energy for the oxidation process was higher than that of the diffusion of oxygen. Hence, it can be concluded that the oxidation process in both the alloys studied is not diffusion controlled.

I. INTRODUCTION

AMONG the various materials and intermetallic compounds that are being considered for high-temperature applications, Ti-Al intermetallic compounds are very promising candidates. This is due to their extraordinary properties such as low density, high-temperature creep resistance, and specific modulus.[1–3] High-temperature oxidation and sulfidation characteristics of Ti-Al based intermetallics with and without ternary alloying additions were studied. It is well known that $TiAl_3$ favors the formation of a continuous a-Al_2O_3 protective scale, while TiAl has lower activation energy for the oxidation and Ti_3Al has very poor oxidation resistance at high temperatures.[4–6] Although $TiAl_3$ forms an alumina layer on oxidation, the brittle nature of the oxide layer owing to the mismatch of thermal expansion coefficients between the base alloy and the oxide has led to the research on oxidation resistance of Ti_3Al intermetallic phase for high-temperature applications. In addition, Ti_3Al has the highest solubility of oxygen,[7] which also stabilizes the α_2 phase. Improvement of high-temperature oxidation resistance of Ti_3Al intermetallic was studied by the addition of elements such as niobium and molybdenum. Oxidation studies of Ti_3Al with various compositions of the microalloying elements and in various environments such as air, pure oxygen, and SO_2 have been investigated.[4–27]

High-temperature oxidation studies on microalloyed Ti_3Al intermetallic with alloying elements such as Mo, Nb, *etc*. were carried out in pure oxygen environment at different temperatures. Although macroalloying was reported to stabilize the Ti_3Al structure, no significant improvement in mechanical properties was observed.[28] In addition, higher amounts of ternary alloy addition lead to formation of oxides of the ternary alloy causing spallation of the oxide layers.[8] Hence, the effect of microalloying of Ti_3Al in its $D0_{19}$ structure with Mo and Nb on the high-temperature oxidation resistance was studied in this research.

Studies on the effect of alloying additions such as Nb and Mo to the Ti_3Al-based alloys on their microstructure and creep resistance were reported in the literature.[29–32] Alloys containing Nb less than 12 at. pct have a two-phase microstructure α_2 (hcp structure based on Ti_3Al) and the high-temperature phase β/B2 (bcc structure). Creep behavior of the Ti_3Al alloys containing 17 at. pct of niobium and at least 1 at. pct of molybdenum were reported. These studies showed that higher Nb content (17 at. pct Nb) in the Ti_3Al alloy demonstrated superior mechanical properties to those containing lower amounts of niobium.

A reaction model to determine the diffusion of oxygen through the oxide scales formed during the oxidation of $TiAl_3$ and Ti_3Al flat sheets is reported in the literature,[4,5] using the Valenci equation and the Pilling–Bedworth ratio. The diffusion of oxygen was calculated using the concentration gradient and the reaction rates. The values of oxygen diffusion reported were different from the values of oxygen diffusion in pure oxides,

M. RAMACHANDRAN and C. WILLIAMS, Graduate Students, D. MANTHA, Research Engineer, and R.G. REDDY, ACIPCO Professor, are with the Department of Metallurgical and Materials Engineering, The University of Alabama, Tuscaloosa, AL 35487. Contact e-mail: rreddy@eng.ua.edu

which was attributed to the nondense and multilayer oxide formed during the oxidation process.

In the present investigation, oxidation studies of Ti_3Al intermetallic with microalloying addition of 2.9 at. pct Mo and 1.1 at. pct Nb in pure oxygen at various temperatures were carried out. The results are analyzed based on the morphological features and orientation of the oxide scales.

II. EXPERIMENTAL PROCEDURE

Ti_3Al microalloyed with either niobium or molybdenum was prepared from 99.999 pct pure titanium rods, 99.99 pct pure aluminum ingots, and 99.9 pct pure molybdenum rods or 99.999 pct pure niobium rods (Alfa Aesar, Ward Hill, MA) by arc melting stoichiometric quantities in a copper crucible under ultra-high-purity argon atmosphere. The surfaces of the microalloyed Ti_3Al ingots were ground and were subsequently heat treated by wrapping in tantalum foil and encasing in quartz tubes at 1273 K (1000 °C) under vacuum for 7 days. The heat-treated ingots were cut into 5 mm × 5 mm × 2 mm tokens and were used in the oxidation studies. A thin piece from each of the sample ingots was sliced and used for X-ray diffraction (XRD) analysis. The intermetallic, Ti_3Al, was microalloyed with 1.1 at. pct Nb and 2.9 at. pct Mo. The prepared samples were oxidized in a ultra-high-purity oxygen atmosphere between temperatures of 1023 K (750 °C) and 1223 K (950 °C) for a time period varying between 24 and 48 hours. The weight gain data were measured using a Perkin Elmer TGA 7 HT, thermogravimetric analyzer (Waltham, MA). The heating rate was 30 K (30 °C) per minute with argon flow in the sample chamber, which was reduced to 5 K (5 °C) per minute closer to the experimental temperature. The gas was changed from argon to ultra-high purity oxygen at the temperature of interest. The samples were cooled in an inert argon atmosphere to room temperature.

The oxidized samples were characterized for phases using a PHILIPS* X-ray diffractometer model PW-1710

---

*PHILIPS is a trademark of Philips Electronics Instruments Inc., Mahwah, NJ.

---

at 40 kV and 35 mA and a monochromated Cu K_α radiation. Morphological features of the oxidized samples were analyzed using a PHILIPS XL30 scanning electron microscope with an attached energy dispersive spectroscope (EDS) for elemental analysis.

III. RESULTS AND DISCUSSION

A. *Oxidation Kinetics*

The weight gain per unit surface area of the alloys as a function of time was obtained from the thermogravimetric analyzer. The oxidation process, as expressed by the weight gain plot, of the Ti-Al intermetallics usually follows one of the parabolic law rate expressions, as

given subsequently. The reaction rate, k_P, can be calculated from the weight gain per unit area, $\Delta W/S$, and time, t.

$$\left(\frac{\Delta W}{S}\right)^2 = k_P t \qquad [1]$$

$$t = A + B\left(\frac{\Delta W}{S}\right) + C\left(\frac{\Delta W}{S}\right)^2 \qquad [2]$$

In Eq. [2], A, B, and C are constants, where C represents the inverse of the parabolic rate constant, k_P. Hence, $k_P = 1/C$. The weight gain per unit surface area *vs* time plots of Ti_3Al-2.9 at. pct Mo and Ti_3Al-1.1 at. pct Nb alloys oxidized in pure oxygen at different temperatures are shown in Figures 1 and 2, respectively. The oxidation curves for the base alloy Ti_3Al in the temperature range of 1023 K to 1223 K (750 °C to 950 °C) are also plotted in the figures. It can be seen that ternary alloying addition of Mo improved the
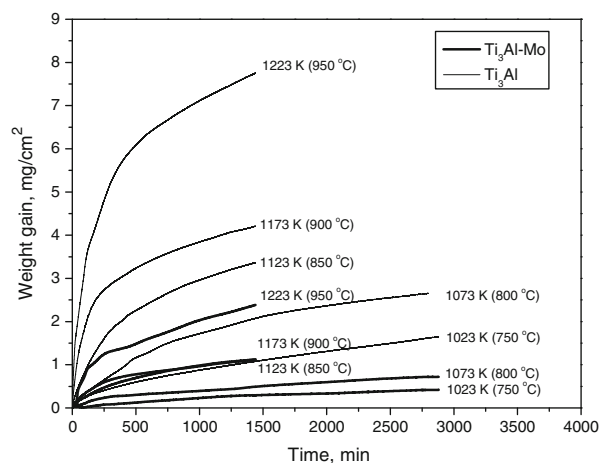

Fig. 1—Weight gain data *vs* time plot for the oxidation of Ti_3Al-2.9 at. pct Mo in pure oxygen atmosphere at various temperatures.
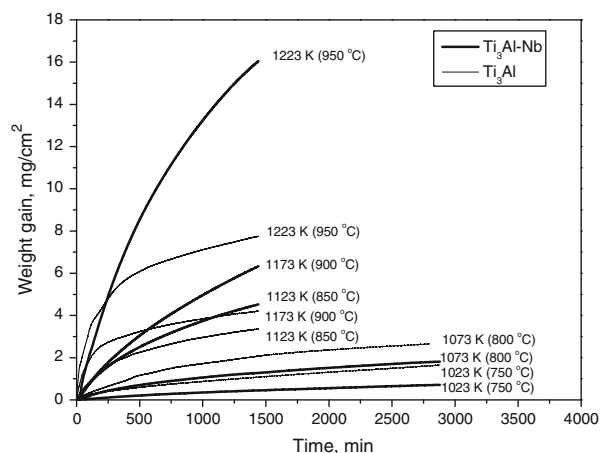

Fig. 2—Weight gain *vs* time plot for the oxidation of Ti_3Al-1.1 at. pct Nb alloy in pure oxygen atmosphere at various temperatures.

oxidation resistance of the base alloy. However, the addition of 1.1 at. pct of Nb to the Ti$_3$Al base alloy did not show improved oxidation resistance at temperatures higher than 1123 K (850 °C). The reason for this behavior could be due to the spallation of the oxide film formed on the alloy surface at higher temperatures that lead to increased oxidation rate. The reaction rate k_P, which is dependent on the temperature, follows an Arrhenius relationship and is given by Eq. [3]:

$$\ln(k_P) = \ln(k_0) - \left(\frac{Q}{R}\right)\left(\frac{1}{T}\right) \quad [3]$$

A plot of $\ln(k_P)$ vs $(1/T)$, as shown in Figure 3, can be used to calculate Q, the activation energy for the oxidation process, from the slope and the reaction rate constant, k_0. It is seen from the plot of $\ln(k_P)$ vs $1/T$ that the reaction rates (k_P) for the oxidation of Ti$_3$Al-1.1 at. pct Nb alloy are higher than those of the Ti$_3$Al-2.9 at. pct Mo alloy. It appears that 2.9 at. pct Mo addition to a Ti$_3$Al intermetallic provides better protection from oxidation in pure oxygen than the addition of 1.1 at. pct Nb. The corresponding activation energy for oxidation for Ti$_3$Al-1.1 at. pct Nb alloy is 295.3 kJ/mol and that of the Ti$_3$Al-2.9 at. pct Mo alloy is 167.8 kJ/mol. The activation energy values obtained in this study are comparable to those obtained in the literature for alloys with similar composition of alloying additions in Table I.
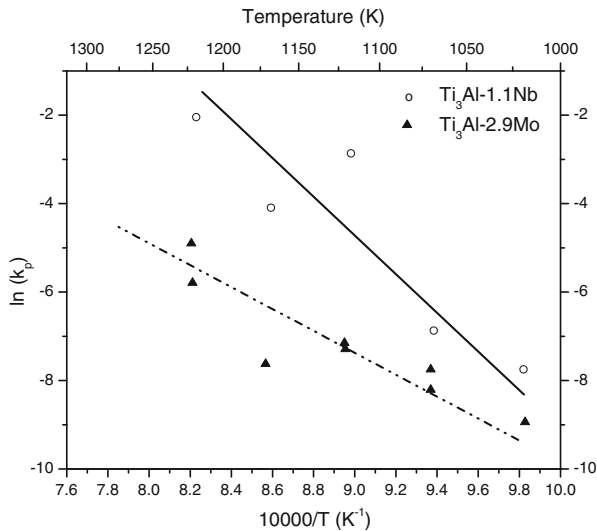
B. Oxide Scale Characterization

The Ti$_3$Al-1.1 at. pct Nb and Ti$_3$Al-2.9 at. pct Mo alloys were oxidized isothermally in pure oxygen at different temperatures from 1023 K to 1223 K (750 °C to 950 °C). The oxide scales formed on the surface of alloys were analyzed for various phases using X-ray diffraction (XRD) and scanning electron microscopy (SEM). The intensities of the peaks help not only to determine the phases present in the oxide scale but also in the determination of crystal orientation and crystal growth in the oxide scale.

The XRD pattern of Ti$_3$Al-2.9 at. pct Mo is shown in Figure 4. The sample oxidized at 1023 K (750 °C) shows the presence of the base metal Ti$_3$Al-2.9 at. pct Mo with small quantities of alumina in the form of corundum. As the temperature is increased from 1073 K to 1123 K (800 °C to 850 °C), the relative quantity of the base metal decreases and the quantity of corundum and TiO$_2$ in its rutile phase increases. A relative amount of corundum formed is maximum at 1123 K (850 °C). On the other hand, the formation of rutile TiO$_2$ increases with an increase in temperature. The orientation of the crystal formed is reflected by the intensities of the diffraction peaks. An analysis of the peak intensities of the base metal at various temperatures shows that its orientation changes with the change in the oxidation temperature, its primary orientation being the [201] plane[33] in the hexagonal primitive structure. This could be explained in terms of the diffusion of individual elements from the bulk of the alloy to the alloy-oxide
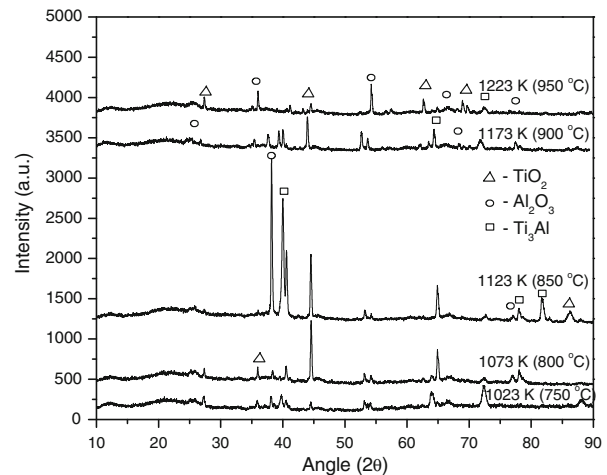

Fig. 3—Ln (k_P) vs 10^4/T for Ti$_3$Al-2.9 at. pct Mo and Ti$_3$Al-1.1 at. pct Nb alloys oxidized in pure oxygen.

Fig. 4—XRD patterns of Ti$_3$Al-2.9 at. pct Mo alloy oxidized at different temperatures.

Table I. Activation Energies of Oxidation in Ti$_3$Al-(Mo/Nb) Alloys in Pure Oxygen

Material	Temperature Range, K (°C)	Activation Energy (kJ/mol)	Reference
Ti$_3$Al-2.9 Mo	1023 to 1223 (750 to 950)	167.8	present study
Ti$_3$Al-2.2 Mo	1073 to 1373 (800 to 1100)	154.9	Livingston et al.[14]
Ti$_3$Al-1.1 Nb	1023 to 1223 (750 to 950)	295.3	present study
Ti$_3$Al-1.34 Nb	1073 to 1373 (800 to 1100)	288.0	Livingston et al.[11]

interface. The corundum formed, on the other hand, has its crystal orientation in the [110] and the [021], while its primary orientation in the rhombohedral rhomb-centered lattice is [104].[33] This variation in the orientation is an effect of the nucleation and growth of these crystals. Rutile (TiO_2) in its tetragonal primitive structure has its close-packed and high intensity plane as [110].[33] However, the orientation of the TiO_2 crystals formed on the oxide scale corresponds mostly to the [200] and the [210] family of planes, which is also mainly due to the nucleation and growth mechanism.

Figure 5 shows the XRD pattern of the Ti_3Al-1.1 at. pct Nb alloy oxidized in pure oxygen in the temperature range of 1023 K to 1223 K (750 °C to 950 °C). The sample oxidized at 1023 K (750 °C) shows the presence of the base metal to be the maximum, indicating that the oxidation is almost negligible. The samples oxidized at higher temperatures, from 1073 K to 1223 K (800 °C to 950 °C), show the presence of Ti_3Al but in relatively lower quantities than the oxides. The XRD patterns of the samples oxidized from 1073 K to 1223 K (800 °C to 950 °C) show the presence of TiO_2 as the major phase in the oxide scale with Al_2O_3 present as a minor phase and approximately at a constant composition.

The orientation of the base metal is in the close-packed plane [201] in the 1023 K (750 °C) sample and changes to the [220] plane with the increase in temperature. The orientation of the TiO_2 crystals remains in the [210] plane at all temperatures, while corundum orients itself in the [012] and [214] planes. Hence, the diffusion of elements in the base metal and the nucleation and growth mechanisms in the oxide scale become important in the determination of the orientation of the oxide scale.

The Ti_3Al-(Mo/Nb) intermetallic alloys were analyzed using SEM for their morphology and particle size distribution after oxidation. Figures 6(a) through (e) show the Ti_3Al-2.9 at. pct Mo alloy oxidized at different temperatures in the range 1023 K to 1223 K (750 °C to 950 °C). Figure 6(a) shows formation of fine-grained
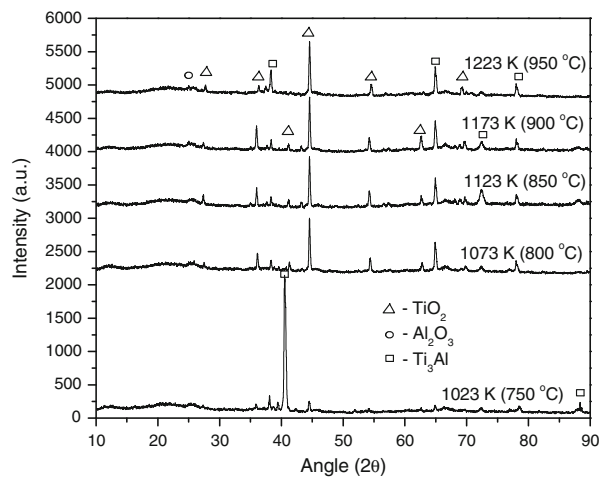
particles with an average particle size of 200 to 300 nm at 1023 K (750 °C). As can be seen from the XRD pattern of this alloy (Figure 4), the micrograph reveals the base metal with particles of TiO_2 and Al_2O_3 spread evenly on its surface. The EDS of this sample (Figure 6 (1)) shows the presence of Ti, Al, and O from the base metal and the oxide scale along with Au, which was used as a coating material. The samples treated at 1073 K, 1123 K, and 1173 K (800 °C, 850 °C, and 900 °C) have an average particle size of 500 nm but form clusters of the oxide scale with its average size varying from 1 to 2 μm. The sample treated at 1223 K (950 °C), in addition to particles of 500 nm in size, forms platelets of average dimensions 15 μm × 5 μm × 500 nm ($L \times W \times T$).

Figures 7(a) through (e) show the Ti_3Al-1.1 at. pct Nb alloy oxidized at different temperatures in pure oxygen. Figure 7(a) shows a similar morphology and particle size as that of the Ti_3Al-2.9 at. pct Mo alloy at 1023 K (750 °C). The average particle size is about 500 nm, and the oxide phase formed is well dispersed on the surface of the base metal. At 1073 K and 1173 K (800 °C and 900 °C), the oxide scale appears to contain fine particles whose average particle size decreases from 2 μm to 500 nm, and at 1223 K (950 °C), the oxide scale contains fine particle clusters with porosity.

Phase analysis was done on the microstructure images obtained from SEM. The contrast of different phases in the micrographs was used to estimate the area fraction of corresponding phases using image analysis software, ImageJ,[34] released by NIH. Assuming the thickness of the oxide layer formed to be uniform in composition, the calculated area fractions equaled the volume fractions. The corresponding mole fractions of different phases in the oxide scale were calculated and given in Table II. The average particle sizes of oxides obtained from the image analyzer lie in the range of about 40 nm to 1 μm for Ti_3Al-2.9 at. pct Mo alloy, which compares well with those observed in the SEM images (500 nm to 2 μm). The particle size range obtained from the image analyzer for the Ti_3Al-1.1 at. pct Nb alloy was 60 to 600 nm, which compares well with those observed in the SEM images (500 nm). As the oxidation temperature increases, the grain size increases due to grain growth. In the Ti_3Al-2.9 at. pct Mo alloy, the variation in the microstructure is observed at 1173 K and 1223 K (900 °C and 950 °C), where fine-grained and plateletlike structures are formed. In the case of Ti_3Al-1.1 at. pct Nb, the average grain size decreases at temperatures above 1123 K (850 °C) but forms clusters of fine particles.

C. Diffusion Analysis

The determination of diffusion coefficients of elements in a given matrix plays a major role in understanding the mechanism of nucleation and growth of crystals. Numerous experimental studies were carried out to understand the diffusion of Ti in various Ti-Al intermetallics.[35] The conventional form of Darken's equation is given in Eq. [4], which relates the interdiffusion coefficient of an alloy AB as a function of intrinsic
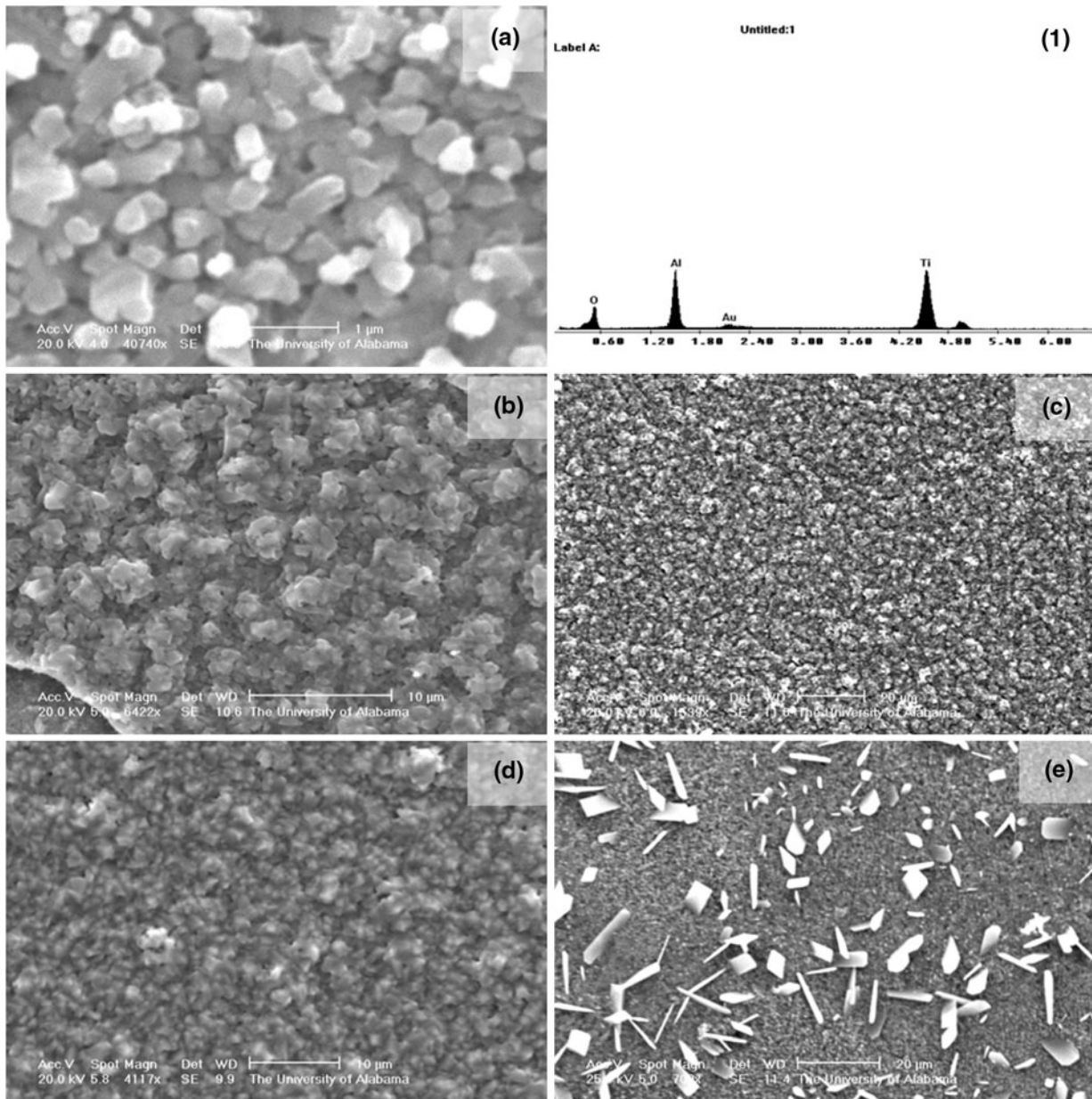
Fig. 5—XRD patterns of Ti_3Al-1.1 at. pct Nb alloy oxidized at different temperatures.

Fig. 6—SEM images of the surfaces of Ti$_3$Al-2.9 at. pct Mo alloy oxidized at (*a*) 1023 K (750 °C), (*b*) 1073 K (800 °C), (*c*) 1123 K (850 °C), (*d*) 1173 K (900 °C), and (*e*) 1223 K (950 °C). EDS of the alloy oxidized at (1) 1023 K (750 °C) is also shown.

diffusivities of individual components (A) and (B) and their atom fractions.

$$\tilde{D} = X_B D_A + X_A D_B \qquad [4]$$

where $\tilde{D}$ represents the interdiffusion coefficient of species A and B in the mixture. The terms X_i and D_i are the atom percent and intrinsic diffusivities of the species, respectively.

In the case of intermetallic compounds, a modified Darken's equation or Darken–Manning equation (Eq. [5]) can be used, which relates the interdiffusion coefficient to the self-diffusivity of elements rather than the intrinsic diffusivity. Experimental determination of self-diffusivity is easier and can be related to the

interdiffusion coefficient by a thermodynamic factor F, as given in Eq. [6]:

$$\tilde{D} = \left(X_B D_A^* + X_A D_B^* \right) \Phi S \qquad [5]$$

where Φ is the thermodynamic factor and S is the vacancy flux effect.

$$\Phi = 1 + \frac{\partial \log \gamma_i}{\partial \log X_i} \quad \text{or} \quad D_i = \left(1 + \frac{\partial \log \gamma_i}{\partial \log X_i} \right) D_i^* \quad [6]$$

where γ is the activity coefficient. $\Phi = 1$ for an ideal system.

The value of Φ for nonideal systems is calculated from their thermodynamic activity data. The vacancy wind
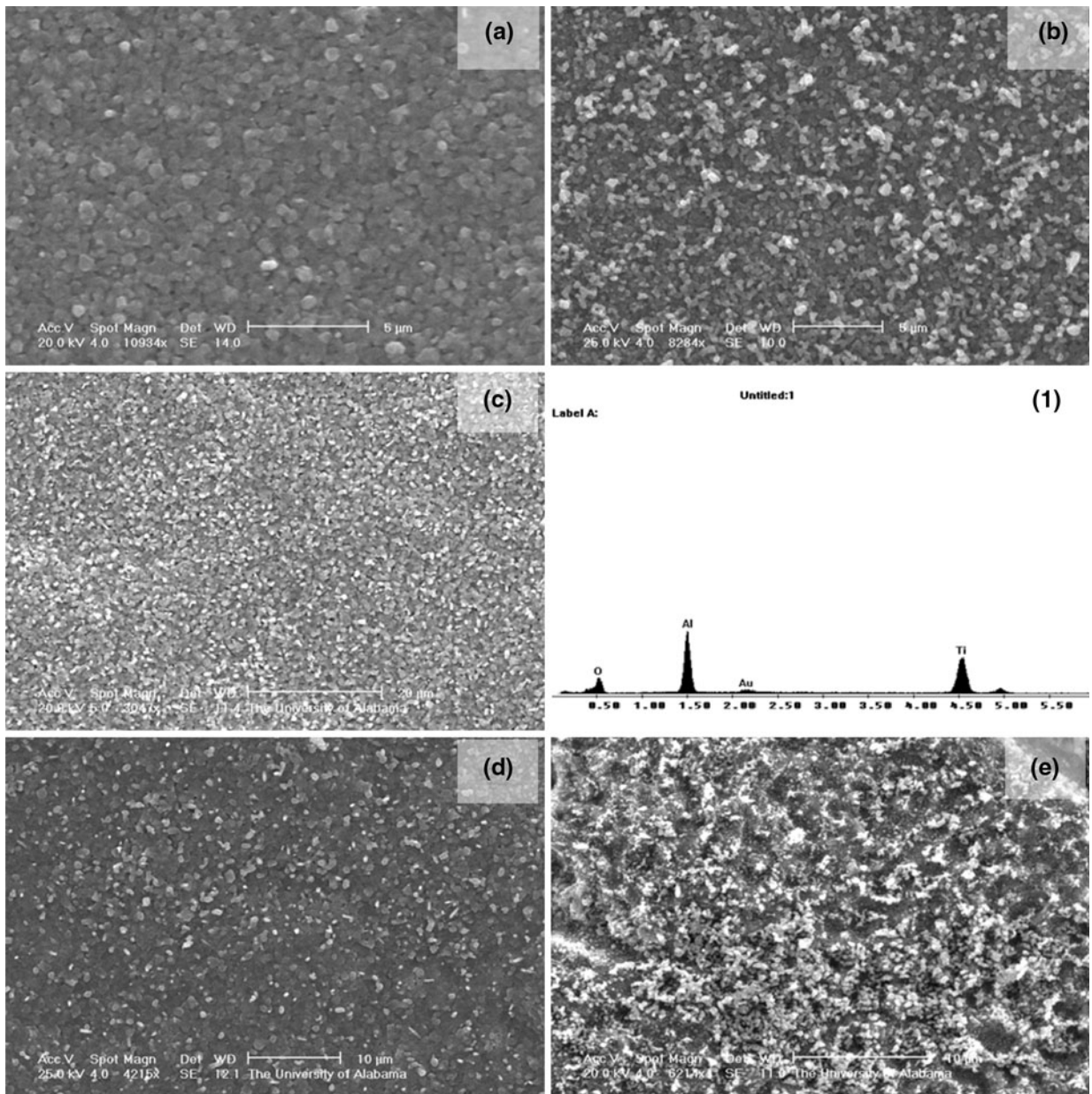
Fig. 7—SEM images of the surfaces of Ti₃Al-1.1 at. pct Nb alloys oxidized in pure oxygen at (*a*) 1023 K (750 °C), (*b*) 1073 K (800 °C), (*c*) 1123 K (850 °C), (*d*) 1173 K (900 °C), and (*e*) 1223 K (950 °C). EDS of the alloy oxidized at 1123 K (850 °C) is also shown (1).

factor, S, is expressed as given in Eq. [7], which is a function of the self-diffusivities, D_i^*, atom fractions, X_i, and a correlation factor, f, for self-diffusion by vacancy mechanism in a pure crystal with a given structure. The value of S can be taken as unity in the intermetallic compound, Ti₃Al, as a first approximation:[39]

$$S = 1 + \frac{(1-f)X_A X_B (D_A^* - D_B^*)^2}{f(X_A D_B^* + X_B D_A^*)(X_A D_A^* + X_B D_B^*)} \quad [7]$$

The values of self-diffusion of Ti in Ti₃Al were calculated using the activation energy for diffusion (Q_{diff}) and diffusivity constant (D_0) obtained from the literature.[36,37] The value of Φ was calculated at

different temperatures using the activity data obtained from FactSage,[40] a thermodynamics database package. Assuming the vacancy wind factor to be unity and ignoring the nonideal conditions in the Darken–Manning equation, the self-diffusion of Al in Ti₃Al was calculated. The calculated values of self-diffusion of aluminum are given in Table III and Figure 8 along with the values of self-diffusion of Ti[36] and interdiffusivity of Ti₃Al[41] reported in the literature. It is seen that the self-diffusion of Al in Ti₃Al is about an order of magnitude less than that of the self-diffusion of Ti and about two orders of magnitude less than that of the interdiffusivity of Ti₃Al at any given temperature. This calculation is in agreement with those reported in the

Table II. Mole Fraction of Various Phases Formed at Different Temperatures

Compound	Temperature, K (°C)	Average Particle Size (nm)	Mole Fraction TiO$_2$	Mole Fraction Al$_2$O$_3$
Ti$_3$Al-2.9 at. pct Mo	1023 (750)	75	0.778	0.222
	1073 (800)	85	0.830	0.170
	1123 (850)	100	0.731	0.269
	1173 (900)	40	0.800	0.200
	1223 (950)	62	0.879	0.121
Ti$_3$Al-1.1 at. pct Nb	1023 (750)	110	0.956	0.044
	1073 (800)	580	0.731	0.269
	1123 (850)	230	0.841	0.159
	1173 (900)	90	0.835	0.165
	1223 (950)	59	0.741	0.259

Table III. Interdiffusion Coefficients D_{Ti_3}Al in Ti$_3$Al,[41] Self-Diffusion of Ti,[36] and Calculated Values of Self-Diffusion of Al

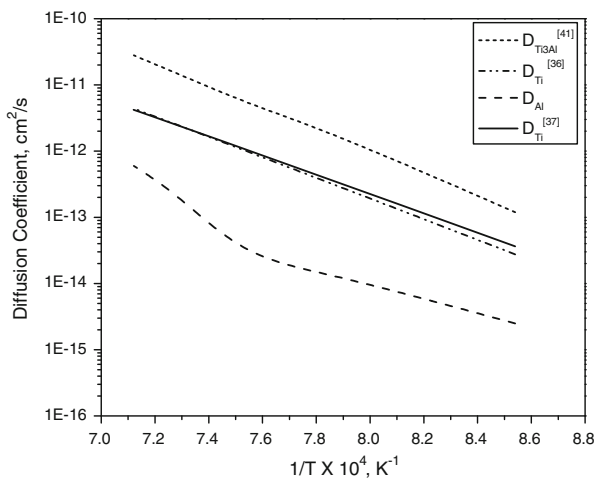| Temperature K (°C)	Interdiffusivity, D_{Ti_3}Al (cm^2/s)[41]	Self-Diffusion of Ti (cm^2/s)[36]	Self-Diffusion of Al (cm^2/s)
1171 (898)	1.2×10^{-13}	2.8×10^{-14}	2.5×10^{-15}
1273 (1000)	1.9×10^{-12}	3.2×10^{-13}	1.4×10^{-14}
1327 (1054)	5.3×10^{-12}	10×10^{-13}	2.4×10^{-14}
1374 (1101)	1.5×10^{-11}	2.5×10^{-12}	2.3×10^{-13}
1404 (1131)	2.8×10^{-11}	4.4×10^{-12}	6.0×10^{-13}

Fig. 8—Interdiffusion coefficient of Ti$_3$Al,[41] self-diffusion of Ti,[36] and the calculated values of self-diffusion of Al.

literature for the self-diffusion of aluminum in Ti$_3$Al.[38] More interestingly, at any given temperature, the variation of self-diffusion of Ti[36] in the aluminum concentration of 25 to 32 at. pct and the variation of interdiffusivity of Ti$_3$Al[41] in the aluminum concentration of 28 to 33 at. pct is very negligible. Hence, from the calculations, it can be concluded that the self-diffusion of aluminum at any given temperature will not vary significantly with the concentration of aluminum in

Table IV. Activation Energies and Diffusion Constant Values for Oxygen Diffusion

Diffusing Material	Activation Energy, Q (kJ/mol)	Diffusion Constant, D_0 (cm^2/s)	Reference
Oxygen in Al$_2$O$_3$	487.2	12.204	Kingery et al.[42]
-do-	337.7	167.2	Reddy et al.[9]
Oxygen in TiO$_2$	246.1	0.994×10^{-3}	Kingery et al.[42]
-do-	295.4	0.68×10^{-4}	Reddy et al.[10]

the composition range of Ti$_3$Al intermetallic phase, which is also substantiated in the literature.[38]

The diffusion of aluminum in pure Ti$_3$Al is relatively slower than that of titanium. The amount of aluminum is about one third that of titanium in the pure Ti$_3$Al phase, and its diffusivity is about an order of magnitude lower than that of titanium. The formation of Al$_2$O$_3$ scale during the oxidation of Ti$_3$Al alloy is relatively difficult. Thermodynamically, the Gibbs energy of formation of Al$_2$O$_3$ is relatively more negative than that of TiO$_2$, and hence, the formation of a protective layer of alumina over the base alloy is controlled mainly by the kinetics of the oxidation reaction.

The effect of the composition of ternary microalloy addition to Ti$_3$Al on its oxidation kinetics was compared to the effective diffusion of oxygen through the oxide layer formed. The diffusivities of oxygen through single-phase oxides (TiO$_2$ and Al$_2$O$_3$) obtained from the literature[42] were compared with those reported for oxygen diffusion in Al$_2$O$_3$[9] and TiO$_2$[10] obtained from the oxidation experiments[9,10] in Table IV. The diffusivities of oxygen in TiO$_2$ and Al$_2$O$_3$ reported in the literature[42] were obtained in oxides that were well sintered and had near-theoretical density. The difference in the diffusivity of oxygen in pure oxides (Al$_2$O$_3$ and TiO$_2$) and those obtained during the oxidation studies is attributed to the morphology and composition of the oxides.

The effective diffusivity of oxygen through the oxide layers is the mole weighted average of the diffusion through individual component. Mathematically,

$$D_{O,eff} = \sum X_i D_{O,i} \qquad [8]$$

where X_i is the mole fraction of individual components and $D_{O,i}$ is the diffusion coefficient of oxygen in a given component. The mole fraction of the oxide scale for this calculation is taken from Table II. The activation energies for oxygen diffusion calculated from the temperature dependence of effective diffusivities of oxygen in Ti$_3$Al-2.9 at. pct Mo and Ti$_3$Al-1.1 at. pct Nb alloys are 24.36 and 23.82 kJ/mol, respectively. The effective diffusivity of oxygen through the oxide scale of the Ti$_3$Al-Mo/Nb alloys shows that the diffusion of oxygen is independent of the type of alloying element.

The effective diffusivity of oxygen through the oxide layers is thus a weaker function of the composition of the oxides in the scale. As can be seen from Table IV, the diffusion of oxygen through TiO$_2$ is faster than that in Al$_2$O$_3$. The higher the amount of TiO$_2$ in the oxide

scale, the faster will be the oxygen diffusion and thus the faster will be the oxidation process. On the other hand, the diffusion of Ti in Al_2O_3 is faster, as reported in the literature,[43] thus forming TiO_2 phase in the oxide scale. The kinetics of the oxidation of Ti and the structure of rutile (TiO_2) together lead to the formation of pores in the oxide scale and, thus, result in spallation of the oxide scale and enable further oxidation of the alloy. This is a similar case with the oxidation of Ti_3Al-2.9 at. pct Mo and Ti_3Al-1.1 at. pct Nb, where the formation of platelets and clusters of fine grains are formed in the oxide scale.

From the present investigation of oxidation of Ti_3Al-2.9 at. pct Mo and Ti_3Al-1.1 at. pct Nb alloys, we can conclude that the formation of TiO_2 is favored with irregular morphology of the oxide layer. A continuous protective layer was not formed in either of these compositions. This is evident from the morphology of the oxide scales obtained during the oxidation studies of the present alloys.

IV. CONCLUSIONS

The oxidation experiments on Ti_3Al-2.9 at. pct Mo and Ti_3Al-1.1 at. pct Nb were carried out in pure oxygen in the temperature range of 1023 K to 1223 K (750 °C to 950 °C). Ti_3Al-2.9 at. pct Mo had better oxidation resistance compared to Ti_3Al-1.1 at. pct Nb. The oxide scale was composed of oxides of aluminum and titanium in various crystallographic orientations. The contrast of the phases in the micrographs was used to calculate the mole fraction of the individual oxides in the oxide scale. The self-diffusion of aluminum in Ti_3Al was calculated using the Darken–Manning equation, and it was found that the self-diffusion of Al was about an order of magnitude less than the self-diffusion of Ti and about two orders of magnitude less than the interdiffusivity of Ti_3Al. The effective diffusion of oxygen in the oxide layers was calculated using the mole fraction of individual oxide and the diffusivity of oxygen in pure oxide. The activation energy for the effective diffusion of oxygen through the oxide layers was determined to be ~24 kJ/mol. The activation energy for the oxidation process was higher than that of the diffusion of oxygen. The oxidation process in both the microalloyed Ti_3Al compositions is chemical reaction controlled rather than diffusion controlled.

REFERENCES

1. J. Subrahmanyam: *J. Mater. Sci.*, 1989, vol. 23, pp. 1906–10.
2. J.L. Smialek: *Scripta Metall. Mater.*, 1992, vol. 26, pp. 1763–68.
3. N. Birks, G.H. Meier, and F.S. Pettit: *JOM*, 1994, vol. 12, pp. 42–46.
4. R.G. Reddy, X. Wen, and C.I. Okafor: *Metall. Trans. A*, 2000, vol. 31A, pp. 3023–28.
5. R.G. Reddy, X. Wen, and I.C. Okafor: *Metall. Trans. A*, 2001, vol. 32A, pp. 491–95.
6. R.G. Reddy, X. Wen, and M. Divakar: *Metall. Trans. A*, 2001, vol. 32A, pp. 2357–61.
7. R.E. Schafrik: *Metall. Trans. B*, 1976, vol. 7B, pp. 713–16.
8. R.G. Reddy: *JOM*, 2002, vol. 54 (2), pp. 65–67.
9. R.G. Reddy, Y. Li, and M.F. Arenas: *High Temp. Mater. Process*, 2002, vol. 21 (4), pp. 195–205.
10. R.G. Reddy, Y. Li, and D. Mantha: *High Temp. Mater. Process*, 2003, vol. 22 (2), pp. 73–85.
11. D. Livingston, D. Mantha, and R.G. Reddy: *High Temp. Mater. Process*, 2006, vol. 25 (3), pp. 121–28.
12. D. Livingston, D. Mantha, and R. G. Reddy: *High Temp. Mater. Process*, 2005, vol. 24 (4), pp. 259–67.
13. C. Williams, D. Mantha, and R.G. Reddy: in *Innovations in Titanium Technology: Microstructure and Properties II*, M.N. Gungor, M.A. Imam, and F.H. Froes, eds., TMS, Warrendale, PA, 2007, pp. 235–44.
14. D. Livingston, D. Mantha, and R.G. Reddy: in *Titanium Alloys for High Temperature Applications—A Symposium Dedicated to the Memory of Dr. Martin Blackburn*, M. Peretti, D. Eylon, U. Habel, and G.C. Keijzers, eds., TMS, Warrendale, PA, 2006, pp. 113–22.
15. G. Welsch and A.I. Kahveci: in *Oxidation of High-Temperature Intermetallics*, T. Grobstein and J. Doychak, eds., TMS, Warrendale, PA, 1988, pp. 207–18.
16. G.H. Meier, D. Appalonia, R.A. Perkins, and K.T. Chiang: in *Oxidation of High-Temperature Intermetallics*, T. Grobstein and J. Doychak, TMS, Warrendale, PA, 1988, pp. 185–93.
17. J.L. Smialek: *Corr. Sci.*, 1993, vol. 35 (5–8), pp. 1199–1208.
18. X. Wen and R.G. Reddy: *Processing and Fabrication of Advanced Materials*, TMS, Warrendale, PA, 1996, pp. 379–89.
19. D. Mantha, X. Wen, and R.G. Reddy: *High Temp. Mater. Process*, 2004, vol. 23 (2), pp. 93–101.
20. K.N. Strafford: *Metall. Rev. (Rev. 138)*, 1969, vol. 14, pp. 153–74.
21. K.N. Strafford and P.K. Datta: *Mater. Sci. Technol.*, 1989, vol. 5, pp. 765–79.
22. S. Mrowec: *High Temp. Mater. Process*, 2003, vol. 22 (1), pp. 1–24.
23. H. Mitsui, H. Habazaki, K. Hashimoto, and S. Mrowec: *Corr. Sci.*, 1997, vol. 39 (1), pp. 59–76.
24. H. Mitsui, H. Habazaki, K. Hashimoto, and S. Mrowec: *Corr. Sci.*, 1997, vol. 39 (1), pp. 9–26.
25. H. Mitsui, H. Habazaki, K. Hashimoto, and S. Mrowec: *Corr. Sci.*, 1997, vol. 39 (9), pp. 1571–83.
26. H. Mitsui, H. Habazaki, K. Asami, K. Hashimoto, and S. Mrowec: *Corr. Sci.*, 1996, vol. 38 (9), pp. 1431–47.
27. H. Habazaki, H. Mitsui, K. Ito, K. Asami, K. Hashimoto, and S. Mrowec: *Corr. Sci.*, 2002, vol. 44, pp. 285–301.
28. D. Banerjee: in *Intermetallic Compounds, Principles and Practice*, J.H. Westbrook and R.L. Fleischer, eds., John Wiley & Sons Ltd., West Sussex, England, 1995, vol. 2, ch. 5, pp. 91–131.
29. J.P. Quast and C.J. Boehlert: *Metall. Mater. Trans. A*, 2007, vol. 38A, pp. 529–36.
30. J.P. Quast and C.J. Boehlert: *J. Mater. Sci.*, 2008, vol. 43, pp. 4411–22.
31. J.W. Zhang, C.S. Lee, D.X. Zou, S.Q. Li, and J.K. L. Lai: *Metall. Mater. Trans. A*, 1998, vol. 29A, pp. 559–64.
32. S. Krishnamurthy, M.R. James, P.R. Smith, and D.B. Miracle: *Proc. 10th Int. Conf. of Composite Materials*, ICCM-10, A. Poursartip and K. Street, eds., Woodhead Publishing Ltd., Vancouver, BC, 1995, vol. II, pp. 739–46.
33. *PCPDFWIN*, Version 2.1, June 2000, JCPDS-ICDD, TiO_2(rutile): 88-1175; TiO_2(anatase): 84-1286; Al_2O_3: 88-0826; and Ti_3Al: 14-0451.
34. W. Rasband: *Image J*, Version 1.41o, National Institutes of Health (NIH), Bethesda, MD.
35. H. Nakajima, W. Sprengel, and K. Nonaka: *Intermetallics*, 1996, vol. 4, pp. S17–S28.
36. J. Rüsing and C. Herzig: *Scripta Metall. Mater.*, 1995, vol. 33 (4), pp. 561–66.

37. C. Herzig, M. Friesel, D. Derdau, and S.V. Divinski: *Intermetallics*, 1999, vol. 7 (10), pp. 1141–51.
38. Y. Mishin and C. Herzig: *Acta Mater.*, 2000, vol. 48, pp. 589–623.
39. T. Shimozaki, Y. Goda, Y. Wakamatsu, and M. Onishi: *Def. Diffus. Forum*, 1993, vols. 95–98, pp. 629–34.
40. *FactSage* 5.11, CRCT, PQ, Canada and GTT, Herzogenrath, Germany.
41. W. Sprengel, H. Nakajima, and H. Oikawa: *Mater. Sci. Eng.*, 1996, vol. A213, pp. 45–50.
42. W.D. Kingery, H.K. Bowen, and D.R. Uhlmann: *Introduction to Ceramics*, 2nd ed., John Wiley & Sons, Inc., New York, NY, 1976, p. 240.
43. Y. Umakoshi, M. Yamaguchi, T. Sakagami, and T. Yamane: *J. Mater. Sci.*, 1989, vol. 24, pp. 1599–1603.